Optics Letters

Differential autocorrelation histogram of singular values for image reconstruction in reflection matrix optical coherence tomography

Lu Yang,[1] Yun Tang,[1] Bingyan Zhang,[1] Changyong Chen,[1] Cui Ma,[1] Zhiyi Liu,[1] and Zhihua Ding[1,2,*]

[1]State Key Laboratory of Extreme Photonics and Instrumentation, College of Optical Science and Engineering, Zhejiang University, Hangzhou 310027, China
[2]ZJU-Hangzhou Global Scientific and Technological Innovation Center, Zhejiang University, Hangzhou 311215, China
*zh_ding@zju.edu.cn

Received 20 March 2025; revised 21 May 2025; accepted 8 June 2025; posted 9 June 2025; published 24 June 2025

Reflection matrix optical coherence tomography has recently emerged as a promising modality for ultra-deep optical imaging in a turbid tissue. However, a critical issue that is not well addressed is to determine the optimized number of primary singular values of the measured reflection matrix used for image reconstruction. In this paper, the method based on the differential autocorrelation histogram of singular values is proposed. The histogram distribution generally consists of two regions with distinct distribution characteristics. One is the continuously distributed region, which is related to the multiple-scattered noise and can be fitted by a skewed distribution curve. The other is the discrete distribution region associated with the single-scattered signal, which does not obey the fitting curve. The boundary between two regions is then identified and used to determine the optimized number of the primary singular values for image reconstruction. Both simulating and experimental results demonstrate that the proposed method is more robust and adaptable to samples with different signal-to-noises and large dynamic ranges of reflectivity, outperforming two currently adopted methods.

https://doi.org/10.1364/OL.563000

Current optical imaging techniques allow non-invasive and rapid assessment of tissue function and structure. However, strong light scattering within biological tissues limits the penetration depth and resolution. Conventional focusing and imaging techniques based on the Born approximation generally fail in strongly scattering media [1,2]. As penetration depth increases, single-scattered (SS) signals attenuate exponentially while multiple-scattered (MS) noise increases sharply, leading to a rapid decrease in the signal-to-noise ratio (SNR) [3]. Recent advances have achieved at least double extension of the penetration depth by the reflection matrix optical coherence tomography (matrix OCT) [2]. This innovative approach combines coherence gating and matrix analysis by the DORT method (French acronym for decomposition of the time reversal operator) to selectively collect the SS signals from the dominant MS noise [2]. Mathematically, the DORT method is equivalent to the singular value decomposition (SVD) of the reflection matrix [4,5]. The SVD processing decomposes the reflection matrix into eigenstates ranked by singular values. The eigenstates with large singular values correspond to relatively high-reflectivity targets [3]. A critical issue in the matrix OCT is to determine the optimized number of primary singular values used to include sufficient eigenstates associated with signals and exclude eigenstates associated with noise.

To determine the optimized number of the primary singular values for image reconstruction, a direct approach is setting a threshold for singular values [6,7]. While this threshold for singular values is seemingly subjective, it can be determined more precisely by finding the maximum value of the ratios to the adjacent singular values [8] or analyzing the differential spectrum of singular values [9]. Besides, the method based on the Shannon entropy of singular values has been tried [10,11]. Moreover, the distribution of the singular values can be exploited. Singular values beyond the superior bound of the empirical distribution of MS contribution are identified as SS signals and selected for image reconstruction [12]. Alternatively, the method based on the quality of the reconstructed image has been applied [2], and the method based on the correlation between image pairs reconstructed from different number of singular values and corresponding remainders has been proposed to achieve reconstructions [13].

Although successful demonstrations have been reported, the robust and adaptive determination of primary singular values for image reconstruction remains a challenge in handling samples with large dynamic range of reflectivity and/or under high noise level. Herein, the method based on the differential autocorrelation histogram of singular values is proposed. Autocorrelation [14–17] and differential operations are combined to enhance the decreasing trend corresponding to SS signals while suppressing the decreasing trend corresponding to MS noise. The enhanced benefits of the operations are the stretching of the SS region and the compression of the MS region in the distribution of the differential autocorrelation coefficients. Subsequently, histogram analysis was further carried out to highlight the distinct

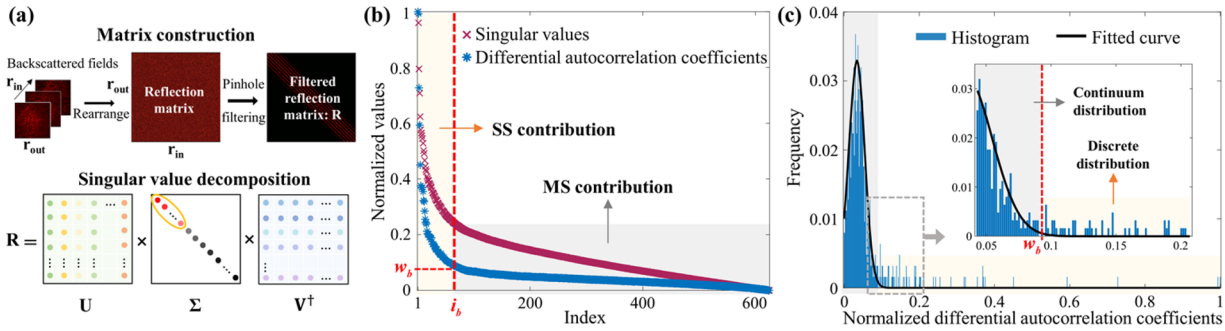

Fig. 1. Schematic of the proposed method. (a) Flow chart of the reflection matrix construction and the SVD processing. r_{in} and r_{out} are the illumination and detection positions. Yellow circle in matrix Σ marks the primary singular values. (b) Distributions of normalized singular values and normalized differential autocorrelation coefficients. Yellow and gray backgrounds mark the SS and MS contributions. Red dotted vertical line marks the optimized number. (c) Histogram distributions and the fitted curve. The continuum and discrete distributions are illustrated with gray and yellow backgrounds. The enlarged view (indicated by the dotted rectangle) shows the red dotted line marking the boundary between two regions.

distribution characteristics associated with SS signals and MS noise, respectively. The continuum distribution (CD) in the histogram associated with MS noise can be fitted to a skewed distribution curve, while the discrete distribution (DD) in the histogram recognized as SS signals does not obey the fitted curve. A boundary between the CD region and the DD region was then identified by a relative deviation analysis and used to determine the primary singular values for optimized image reconstruction. To confirm the enhanced performance of the proposed method, image reconstructions were done on simulated and experimental samples with different SNRs and varying dynamic ranges of reflectivity by the developed method and two existing methods.

The flow chart of the reflection matrix construction and the SVD processing is depicted in Fig. 1(a). The measured backscattered fields corresponding to different focused illumination positions were reshaped into column vectors and arranged in the reflection matrix in the order of the scanning trajectory [2]. A digital pinhole was adopted to filter out the off diagonal elements associated with MS noise to obtain a filtered reflection matrix R. To remove residual MS contribution, SVD processing of R was performed. The SVD processing and image reconstruction [2] are expressed as $R = U\Sigma V^{\dagger}$ and $I = \sum_{i=1}^{M} \sigma_i |\widetilde{U}_i \circ \widetilde{V}_i|$, where, the superscript † stands for transpose conjugate and ∘ represents the Hadamard product. U and V are unitary matrices whose columns are the input and output singular vectors U_i and V_i. $\widetilde{U}_i$ and $\widetilde{V}_i$ are two-dimensional matrices reshaped from U_i and V_i according to the scanning trajectory [18]. Σ is a diagonal matrix consisting of the real positive singular values σ_i in a decreasing order of index $i\{i \in [1, N]\}$, with N being the size of Σ, and M ($M < N$) is the optimized number of the primary singular values used for the optimized image reconstruction.

Considering that the analytical model of singular value distribution is difficult or even impossible to establish, we take the experimental distribution obtained from a measured reflection matrix as the basis for subsequent analysis. As shown in Fig. 1(b), except for a few discrete high singular values undoubtedly related to SS signals, the remaining low singular values are difficult to separate from a continuum of low singular values associated with MS noise, consistent with [19]. To realize a robust and adaptable separation of the singular values corresponding to SS signals and MS noise, we modify the distribution of the singular values with the differential autocorrelation operations expressed by $c_i = \sum_{j=1}^{N-i+1} \sigma_j \times \sigma_{j+i-1}$ and $w_i = c_i - c_{i+1}$, where c_i and w_i are the autocorrelation coefficient and the differential autocorrelation coefficient with the subscript i as the index in the sequence of singular values in a decreasing order. As shown in Fig. 1(b), the differential autocorrelation operations intensify the descending trend of the SS contribution but suppress this trend of the MS contribution. To further differentiate the distribution characteristics, histogram distribution $h(w)$ of the differential autocorrelation coefficients was calculated with the number of bins equal to the size of Σ. From Fig. 1(c), $h(w)$ exhibits two regions with distinguishable distribution characteristics: a CD region of low coefficients with peak-shaped high frequency and a DD region of high coefficients with low frequency. The CD region can be fitted with a skewed distribution curve $f(w)$, approximated by the combination of two different normal distributions with distinct variances expressed by

$$f(w) = \begin{cases} m \cdot \exp\left(-\frac{(w-w_c)^2}{2v_l^2}\right), & w_{\min} \le w < w_c \\ m \cdot \exp\left(-\frac{(w-w_c)^2}{2v_r^2}\right), & w_c \le w < w_{\max} \end{cases}, \quad (1)$$

where $w_{\min}$ and $w_{\max}$ are the minimum and the maximum differential autocorrelation coefficients, w_c is the differential autocorrelation coefficient corresponding to the centroid within the full width at half maximum range of the CD region, m is the average of top ten frequencies, and the standard deviations v_l and v_r are obtained by nonlinear least squares fitting.

To better visualize the different distributions of the CD and DD regions, an enlarged view of the dotted rectangular area is displayed in Fig. 1(c), where the frequency of $f(w)$ decreases rapidly to almost zero with increased differential autocorrelation coefficients. Initially, continuous bars consistent with $f(w)$ are demonstrated. However, as the differential autocorrelation coefficient increases, discrete bars with large deviations from $f(w)$ are presented. In other words, the DD region does not follow $f(w)$ and is readily to be separated from the CD region. To determine the boundary between two regions, the relative deviation was calculated as $\varepsilon(w) = |h(w) - f(w)|/f(w)$ and employed to identify the boundary using a preset threshold of $\varepsilon_t = 5$, along with histogram distribution-dependent adjustments for different tissue types and imaging conditions (Supplement 1). Once the boundary (red dotted vertical line in Fig. 1(c)) between two regions is determined, the corresponding coefficient w_b as well as the optimized number $M = i_b$ (red dotted vertical line in Fig. 1(b)) is thus determined.

To demonstrate the adaptability of the proposed method to the SNR and the dynamic range of reflectivity, simulations were carried out [13,20]. First, a reference sample composed of six bars with different added noise was simulated to study the dependence of the histogram distribution on the SNR. MS contribution was modeled as additive Gaussian noise [4,13]. Second, 10 groups of reference samples consisting of six vertical bars with fixed reflectivity of 0.1 and one horizontal bar with reflectivity varied from 0.1 to 1 (under the same added noise as that in the first case of Fig. 2(a)) were simulated to study the dependence of histogram distribution on the dynamic ranges of reflectivity. Figure 2(a) shows the corresponding results of three typical cases with SNRs of −29.5 dB, −34.5 dB, and −39.5 dB, respectively. Confocal images and reconstructed images by the proposed method were also presented. As SNR decreases, the confocal image becomes blurred and invisible. Correspondingly, the histogram distribution progressively narrows, converging to smaller coefficients and increasingly approximating that of the matrix containing only MS noise (simulated as a Gaussian random matrix with zero mean and variance 1) [4,12]. For the random matrix, the fitted curve shows good agreement with the histogram distribution, with no observed DD region (Fig. 2(b)). Meanwhile, the number of coefficients decreases in the DD region and increases in the CD region, consistent with the decrease in the number of primary singular values related to SS signals and the increase in the number of singular values related to MS noise. The dependence of the coefficients within the DD region versus the SNR is detailed in Fig. 2(c). With the decrease of the SNR, the maximum value of the coefficient decreases and the minimum value increases, resulting in the narrowing of the DD region. Figure 2(d) illustrates the dependence of the coefficients within the DD region versus the increasing dynamic ranges of reflectivity. With the increase of the dynamic range of reflectivity, the maximum value of the coefficient increases and the minimum value of the coefficient decreases, resulting in the broadening of the DD region. Since the noise added in simulation is the same, the increase in the dynamic range of reflectivity is equivalent to the increase in the SNR. Therefore, the coefficient within the DD region shows a similar dependence on the dynamic range of reflectivity as that on the SNR. This simulated study confirms the adaptability of the histogram distribution and its fitted curve to varying SNRs and dynamic ranges of reflectivity, allowing robust discrimination of the DD region for image reconstruction.

To demonstrate the enhanced performance of the proposed method over two existing methods, image quality evaluations based on image similarity were conducted in simulations. The structural similarity index (SSIM) [21] was introduced to evaluate image similarity between reconstructed images and their references. The entropy method [11] and the correlation method [13] were taken as two typical existing methods for comparison. Figure 3 shows the results on similarity versus SNRs and dynamic ranges of reflectivity obtained by the three methods. In Fig. 3(a), the reference sample was the same as that adopted in Fig. 2(a), and 10 groups of cases (Group 1–10) were simulated with decreasing SNRs ranging from −29.5 dB to −38.5 dB with −1 dB decrements between successive groups. In Fig. 3(b), the reference samples and noise were the same as those used in Fig. 2(d). The entropy method, which uses a fixed threshold to select singular values retaining a certain percentage of entropy, is only effective in the case of high SNR and uniform reflectivity. The correlation method is robust to different SNRs but fails in

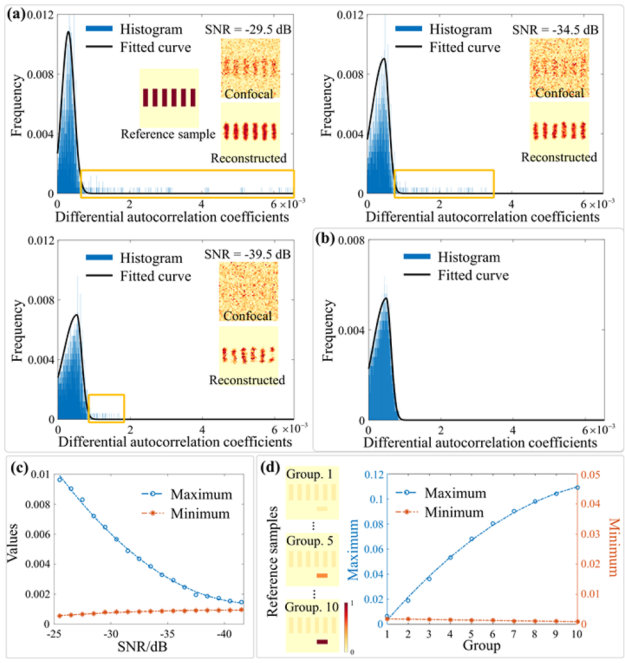

Fig. 2. Adaptability of the proposed method to SNRs and dynamic ranges of reflectivity. (a) Histogram distribution for three typical cases with decreasing SNRs. Yellow rectangles mark the DD regions. (b) Histogram distribution for the random matrix. (c) Coefficients within the DD region versus the SNR. (d) Coefficients within the DD region versus the group number corresponding to the increasing dynamic range of reflectivity.

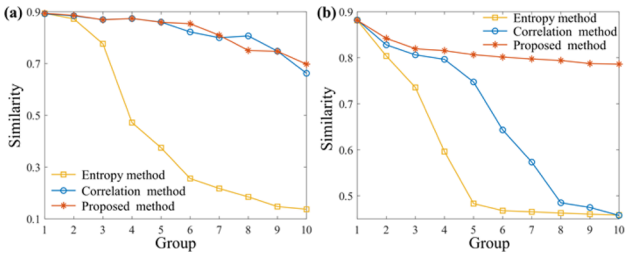

Fig. 3. Similarity of image reconstructed by three methods under different SNRs (a) and varying dynamic ranges of reflectivity of the samples (b).

samples with large dynamic ranges of reflectivity, as such image-based approach tends to emphasize high-reflectivity components and ignore low-reflectivity ones. In comparison, the proposed method is robust at different SNRs and varying dynamic ranges of reflectivity of the sample, outperforming both of the existing methods.

To demonstrate the feasibility of the developed method to general biological sample, reflection matrices were measured, and image reconstructions were conducted. A matrix OCT system similar to that described in [2] was established, and the lateral and axial resolutions were calibrated to be 15 μm and 10 μm, respectively. The sample under imaging is fresh juice vesicles from a citrus fruit. Figure 4 shows the reconstructed en face images corresponding to varying imaging depths (different SNRs) and different areas (with different dynamic ranges of reflectivity). Confocal images were also constructed for reference. The entropy method only achieves faithful reconstruction

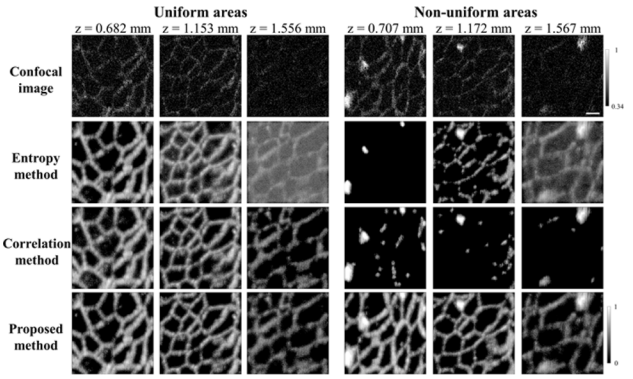

Fig. 4. Reconstructed images of biological sample by different methods. z indicates the imaging depth from the upper surface. Scale bar, 100 μm.

at shallow depth for areas with uniform reflectivity but fails at deeper depths and non-uniform areas with large dynamic ranges of reflectivity. The correlation method can realize robust reconstruction for uniform areas even at the deepest depth but fails in non-uniform areas with large dynamic ranges of reflectivity. In comparison, the proposed method provides robust reconstructions through the imaging depths and is applicable to both uniform and non-uniform areas. Furthermore, the proposed method achieves relatively high computational efficiency (less than 0.08 s), with quantitative comparisons provided in Supplement 1.

In summary, the proposed method determines the optimized number of primary singular values for high-quality image reconstruction using differential autocorrelation histogram analysis of singular values. However, the reflectivity of the sample also has a non-negligible influence on singular values. The distinction between SS signals and MS noise may be not clear in highly heterogeneous biological samples, resulting in artifacts or incomplete reconstructions. Although the proposed method achieves robust and adaptive image reconstructions of samples with different SNRs and dynamic ranges of reflectivity, it can be refined if the reflectivity distribution of the sample is further taken into consideration in the isolation of SS signals from MS noise.

Funding. National Natural Science Foundation of China (62035011, 31927801, 11974310, 62275232).

Disclosures. The authors declare no conflicts of interest.

Data availability. The data that support the findings of this study are available from the corresponding authors upon request.

Supplemental document. See Supplement 1 for supporting content.

REFERENCES

1. A. Badon, A. C. Boccara, G. Lerosey, *et al.*, Opt. Express **25**, 28914 (2017).
2. A. Badon, D. Li, G. Lerosey, *et al.*, Sci. Adv. **2**, e1600370 (2016).
3. S. Yoon, M. Kim, M. Jang, *et al.*, Nat. Rev. Phys **2**, 141 (2020).
4. A. Aubry and A. Derode, Waves Random Complex Medium **20**, 333 (2010).
5. C. Prada, S. Manneville, D. Spoliansky, *et al.*, J. Acoust. Soc. Am. **99**, 2067 (1996).
6. K. Konstantinides and K. Yao, IEEE Trans. Acoust. Speech Signal Process **36**, 757 (1988).
7. Q. Yang, Y. Miao, T. Huo, *et al.*, Appl. Phys. Lett **113**, 011106 (2018).
8. M. B. Roumeliotis, R. Z. Stodilka, M. A. Anastasio, *et al.*, Opt. Express **19**, 13405 (2011).
9. X. Zhao and B. Ye, Mech. Syst. Sig. Process. **25**, 1617 (2011).
10. A. Badon, V. Barolle, K. Irsch, *et al.*, Sci. Adv. **6**, eaay7170 (2020).
11. O. Alter, P. O. Brown, and D. Botstein, Proc. Natl. Acad. Sci. **97**, 10101 (2000).
12. A. Aubry and A. Derode, J. Appl. Phys. **106**, 044903 (2009).
13. L. Yang, T. Han, J. Meng, *et al.*, Opt. Express **30**, 2680 (2022).
14. P. J. Brockwell and R. A. Davis, *Introduction to Time Series and Forecasting* (Springer, 2002).
15. K. Kikuchi and T. Nanahara, in *2014 49th International Universities Power Engineering Conference (UPEC)* (IEEE, 2014), pp. 1–5.
16. M. S. B. Sinal and E. Kamioka, J. Comput. Commun. **6**, 63 (2018).
17. W. Xu, Y. Shen, Q. Jiang, *et al.*, Meas. Sci. Technol. **33**, 085112 (2022).
18. Q. Yang, J. Cao, Y. Miao, *et al.*, Opt. Lett **45**, 828 (2020).
19. S. M. Popoff, A. Aubry, G. Lerosey, *et al.*, Phys. Rev. Lett **107**, 263901 (2011).
20. S. Yoon, H. Lee, J. H. Hong, *et al.*, Nat. Commun **11**, 5721 (2020).
21. A. Horé and D. Ziou, in *2010 20th International Conference on Pattern Recognition* (2010), pp. 2366–2369.